NONLINEAR ANALYSIS
MODELLING AND CONTROL

Nonlinear Analysis: Modelling and Control
ISSN: 1392-5113
ISSN: 2335-8963
nonlinear@mii.vu.lt
Vilniaus Universitetas
Lituania

Dynamic analysis of a Leslie–Gower-type predator–prey system with the fear effect and ratio-dependent Holling III functional response

Chen, Hongyu; Zhang, Chunrui

Dynamic analysis of a Leslie–Gower-type predator–prey system with the fear effect and ratio-dependent Holling III functional response
Nonlinear Analysis: Modelling and Control, vol. 27, núm. 5, 2022
Vilniaus Universitetas, Lituania
Disponible en: https://www.redalyc.org/articulo.oa?id=694173273005
DOI: https://doi.org/10.15388/namc.2022.27.27932

Dynamic analysis of a Leslie–Gower-type predator–prey system with the fear effect and ratio-dependent Holling III functional response

Hongyu Chen chenhongyu19982021@163.com
Northeast Forestry University, China
Chunrui Zhang
Northeast Forestry University, China

Abstract: In this paper, we extend a Leslie–Gower-type predator–prey system with ratio-dependent Holling III functional response considering the cost of antipredator defence due to fear. We study the impact of the fear effect on the model, and we find that many interesting dynamical properties of the model can occur when the fear effect is present. Firstly, the relationship between the fear coefficient K and the positive equilibrium point is introduced. Meanwhile, the existence of the Turing instability, the Hopf bifurcation, and the Turing–Hopf bifurcation are analyzed by some key bifurcation parameters. Next, a normal form for the Turing–Hopf bifurcation is calculated. Finally, numerical simulations are carried out to corroborate our theoretical results.

Keywords: predator–prey system, the fear effect, Turing instability, Turing–Hopf bifurcation, normal form.

Nonlinear Analysis: Modelling and Control, vol. 27, núm. 5, 2022

Vilniaus Universitetas, Lituania

Recepción: 03 Noviembre 2021
Revisado: 23 Abril 2022
Publicación: 29 Junio 2022

DOI: https://doi.org/10.15388/namc.2022.27.27932

Redalyc: https://www.redalyc.org/articulo.oa?id=694173273005

1 Introduction

As one of the most common mutual relationships between two populations in nature, predator–prey relationship plays a significant role in ecology and mathematical biology [2]. Since the dynamic behaviours of predator–prey models were formulated by Lotka and Volterra, many experts and scholars have studied various types of predator–prey models over the past decades, thus establishing the theoretical basis for interspecific interactions [1, 4, 12, 14]. In 1948, Leslie and Gower introduced a functional response called Leslie– Gower, which was based on the Logistic model proposed by Verhulst. This functional response can be adapted to describe the correlation between a reduction in the number of predators and the per capita availability of the predator's preferred food [2, 17]. The Leslie–Gower predator–prey system typically takes the following form:

$$\frac{\mathrm{d}x}{\mathrm{d}t} = rx\left(1-\frac{x}{K}\right) - yf(x), \qquad \frac{\mathrm{d}y}{\mathrm{d}t} = y\left(1-\frac{y}{px}\right),$$
$$x(0) > 0, \quad y(0) > 0, \quad r, s, K, p > 0, \tag{1}$$

where p is the prey-to-predator conversion factor, and the term $y/(px)$ is known as the Leslie–Gower term, which means the scarcity of prey leads to a loss of predator density.

The functional response is an important component of the predator–prey model describing the way in which predator–prey interactions occur. In proposing this function, an essential role is played by the behavior of prey and predator [17,18]. Some common types of functional responses are listed here. For example, Holling I–III functional response [20], Beddington–DeAngelis functional response [10], Leslie–Gower functional response [11], Crowley–Martin functional response [9], and ratio-dependent functional response [6].

The ratio-dependent functional response, a predator-dependent functional response, is an important form in characterizing the functional responses of predator and has a better modeling for a predator–prey system [25]. Based on the existed studies and the above considerations, many experts and scholars have replaced $f(x)$ in (1) with a ratio-dependent functional response and considered its spatial distribution patterns and dispersal mechanisms. Making a suitable nondimensional scaling, system (1) reduces to

$$\begin{aligned}\frac{\partial u(x,t)}{\partial t} &= d_1\Delta u + u(1-u) - \frac{\beta u^2 v}{u^2+mv^2},\\ \frac{\partial v(x,t)}{\partial t} &= d_2\Delta v + rv\left(1-\frac{v}{u}\right),\end{aligned} \tag{2}$$

where $u(x,t)$ and $v(x,t)$ denote, respectively, the densities of the prey and the predator species at the space location x and time t. Δ is the Laplacian operator. The positive constants d_1 and d_2 represent separately the diffusion coefficients of the prey and the predator. Parameters$r$, m, and β are all positive constants. The nonlinear term $\beta u^2/(u^2+mv^2)$ in (2) is called ratio-dependent Holling type III functional response [5, 21], and it indicates the growth rate of predator per capita, which is a function of the ratio of the number of prey to predator. The term v/u is known as the Leslie–Gower term [8], and it means the scarcity of prey leads to a loss of predator density [16]. There have been several reports on the dynamic behavior of this ratio-dependent predator–prey system (2). The Turing and Turing–Hopf bifurcations of system (2) were investigated and the spatiotemporal patterns of system (2) in two-dimensional space were discovered by Chen and Wu [3]. In [16], under homogeneous Neumann boundary conditions, the existence conditions of Hopf bifurcation, Turing instability of spatial uniformity and Turing–Hopf bifurcation in one- dimensional space were shown. In Chang and Zhang [2], they used the Leray–Schauder degree theory and the implicit function theorem to report the nature of the spatially homogeneous Hopf

bifurcation and the nonexistence and existence of nonconstant steady states.

In proposing model (2), the fear effect of prey for predator has been neglected. All prey respond to the risk of predation and then exhibit a variety of antipredator responses. The common ones are habitat change, foraging, vigilance, and other different physiological changes [15,19,22–24]. Some previous experimental studies have confirmed this result. In addition, the fear of predation has immense impact on prey species. The mortality of prey is directly increased by predation. Moreover, the fear of prey may affect the physiological condition of juvenile prey, which is harmful to its survival in adulthood, for example, reducing the reproduction of prey [19, 22]. Furthermore, strong behavioral responses can be elicited by the fear of predation enough to affect the population and life history of entire prey populations [13]. According to their ideas [22–24], we extend model (2) by multiplying the production term by a factor $f(K,v)=1/(1+Kv)$ taking in account the cost of antipredator defence due to fear [22], then model (2) becomes

$$\begin{aligned}
&\frac{\partial u(x,t)}{\partial t} = d_1\Delta u + \frac{u}{1+Kv} - u^2 - \frac{\beta u^2 v}{u^2+mv^2}, \quad x\in\Omega,\ t>0,\\
&\frac{\partial v(x,t)}{\partial t} = d_2\Delta v + rv\left(1-\frac{v}{u}\right), \quad x\in\Omega,\ t>0,\\
&u_x(x,t) = v_x(x,t) = 0, \quad x\in\partial\Omega, \quad t>0,\\
&u(x,0) = u_0(x)\geqslant 0, \quad v(x,0) = v_0(x)\geqslant 0, \quad x\in\overline{\Omega},
\end{aligned} \tag{3}$$

where parameter $K>0$ refers to the level of fear.

The organizational structure of this paper is as follows. In Section 2, both the existence of positive equilibrium state and the linear stability of system (3) are analysed. Further-more, the bifurcation analysis is investigated in Section 3, where the existence of the Turing bifurcation, the Hopf bifurcation, and the Turing–Hopf bifurcation are shown by choosing the d_2, r, and K as bifurcation parameters, respectively. Moreover, the normal form of the Turing–Hopf bifurcation with r and d_2 as parameters for system (3) near the unique positive constant equilibrium is obtained in Section 4. Finally, in Section 5, numerical simulations are carried out to verify the obtained theoretical conclusions.

2 Existence and stability of equilibria

Firstly, the existence of coexisting equilibrium is analyzed by considering the following equation:

$$f(u,v)=\frac{u}{1+Kv}-u^2-\frac{\beta u^2 v}{u^2+mv^2}=0,$$
$$g(u,v)=rv\left(1-\frac{v}{u}\right)=0. \tag{4}$$

Obviously, (1, 0) is a boundary equilibrium point of system (3). In this article, we mainly study the relevant properties of the coexistence equilibrium of system (3). By using the second equation of (4), we are able to obtain $u=v$. Substituting this into the first equation of (4), we obtain the expression $h(u)=-K(1+m)u^2-(1+m+K\beta)u+(1+m-\beta)$.

Theorem 1. *The following statements are correct*:

i. Assume that $1+m-\beta>0$ holds, then $h(u)=0$ must have a positive real solution.
ii. The equilibrium of prey u_* is a strictly decreasing function with respect to K when $1+m-\beta>0$.

Proof. (i) Obviously, $h(u)$ is a quadratic function of one variable u with the downward opening, and its symmetry axis is $u=-(1+m+K\beta)/(2K(1+m))<0$. We can also find $h(0)=1+m-\beta$. So there must be a positive solution u_* to meet $h(u_*)=0$ when $1+m-\beta>0$.

(ii) In the case with the fear factor, i.e., $K>0$, for system (3), when $1+m-\beta>0$., we can obtain the equilibrium of prey

$$u_*=\frac{-1-m-K\beta+\sqrt{4(K+Km)(1+m-\beta)+(1+m+K\beta)^2}}{2(K+Km)}.$$

Simple computation shows

$$\frac{\mathrm{d}u_*}{\mathrm{d}K}=\frac{-1-2K-m-2Km+K\beta+\sqrt{4(K+Km)(1+m-\beta)+(1+m+K\beta)^2}}{2K^2\sqrt{4(K+Km)(1+m-\beta)+(1+m+K\beta)^2}}<0,$$

that which indicates that u_* is a strictly decreasing function with respect to K. That is, increasing the level of K can decrease the value of the prey equilibrium u_*.

Theorem 1 means that system (3) has a positive equilibrium point. We suppose that (u_*,v_*) is the positive equilibrium point of system (3) for the remainder of the article. Furthermore, it also means that if the model has a unique positive equilibrium, the fear coefficient K has an effect on the positive equilibrium point: as the fear coefficient K increases, the positive equilibrium point of prey u_* gradually decreases (see Fig. 1). Next, we conduct a linear stability analysis of system (3). For the positive equilibrium (u_*,v_*), the linearized system of (3) is

$$\begin{pmatrix} u_t \\ v_t \end{pmatrix} = D \begin{pmatrix} \Delta u \\ \Delta v \end{pmatrix} + L \begin{pmatrix} u \\ v \end{pmatrix}, \tag{5}$$

where

$$D = \begin{pmatrix} d_1 & 0 \\ 0 & d_2 \end{pmatrix}, \qquad L = \begin{pmatrix} a_1 & a_2 \\ r & -r \end{pmatrix},$$

and

$$a_1 = -2u_* + \frac{1}{1+Ku_*} - \frac{2m\beta}{(1+m)^2}, \qquad a_2 = -\frac{Ku_*}{(1+Ku_*)^2} + \frac{(m-1)\beta}{(1+m)^2}.$$

It is obvious to know that the characteristic equation of the linearized system (5) is

$$\lambda^2 - \mathrm{TR}_n\,\lambda + \mathrm{DET}_n = 0, \quad n \in N_0, \tag{6}$$

where

$$\mu_n = \frac{n^2}{l^2}, \qquad \mathrm{TR}_n = -(d_1+d_2)\mu_n - r + a_1,$$

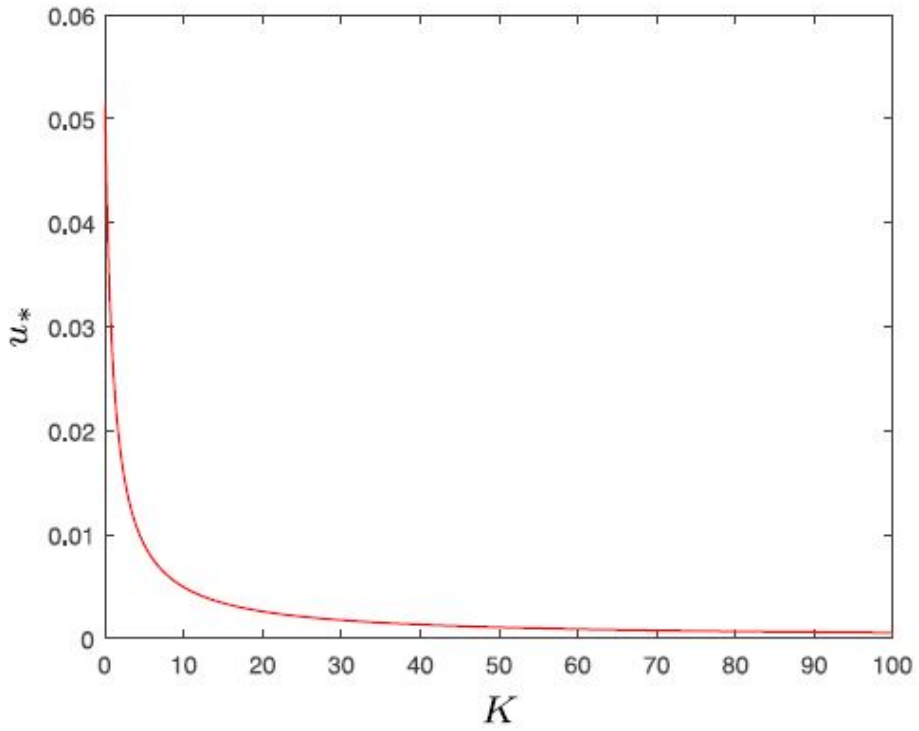

Figure 1
Curve of relationship between K and u#. Keeping the other parameters fixed at the values: m = 0.35, β = 1.28.

$$\mathrm{DET}_n = d_1 d_2 \mu_n^2 + (d_1 r - a_1 d_2)\mu_n - (a_1 + a_2) r, \tag{7}$$

and the eigenvalues of system (3) are given by

$$\lambda_{1,2}^{(n)} = \frac{\mathrm{TR}_n \pm \sqrt{\mathrm{TR}_n^2 - 4\,\mathrm{DET}_n}}{2}, \quad n \in N_0. \tag{8}$$

Then we make the following hypotheses:

$$\text{(A1)}\ \ a_1 - r < 0;$$
$$\text{(A2)}\ \ a_1 + a_2 < 0.$$

If Assumptions (A1) and (A2) are both valid, then when $n = 0$, there is $\mathrm{TR}_0 < 0$ and $\mathrm{DET}_0 > 0$, that is to say, the real parts of the eigenvalues of system (3) are all less than zero. Therefore, the following theorem is obtained.

Theorem 2. *Suppose that* (A1) *and* (A2) *hold. Then the ordinary differential equation system corresponding to system* (3) *is locally asymptotically stable at the positive equilibrium point* (u_*, v_*).

3 Bifurcation analysis

3.1 Turing instability

In this section, the existence conditions of the Turing instability are analyzed. Under the assumptions that (A1) and (A2) are established, it is known from Theorem 2 that there is $\mathrm{TR}_n < \mathrm{TR}_0 < 0$ for $n \in N_0$. Then d_2 (see (7)) is selected as the Turing bifurcation line parameter. Let $a_1 > 0$ and discuss in the following three situations:

Case 1. $d_2 \leqslant d_1 r/a_1$,

Case 2. $d_2 \leqslant d_1 r/a_1$, and $\Delta < 0$, where $\Delta = (d_1 r - a_1 d_2)^2 + 4 d_1 d_2 (a_1 + a_2) r$,

Case 3. $d_2 \leqslant d_1 r/a_1$, and $\Delta < 0$, where $\Delta = (d_1 r - a_1 d_2)^2 + 4 d_1 d_2 (a_1 + a_2) r$,

After the analysis and discussion of the above three situations, we can get the following theorem.

Theorem 3. *Suppose* (A1) *and* (A2) *hold. Then the following statements are correct*:

i. In Case 1 or Case 2, the positive equilibrium point (u_*, v_*) is locally asymptotically stable.
ii. In Case 3, if there does not exist a $\mu_n (n \in N_0)$ such that $\mathrm{DET}_n < 0$, then the positive equilibrium point (u_*, v_*) of system (3) is locally asymptotically stable; conversely, if there exists at least a $\mu_n (n \in N_0)$ such that $\mathrm{DET}_n < 0$, then the positive equilibrium point (u_*, v_*) of system (3) is Turing unstable

Proof. Suppose that (A1) and (A2) hold. Under the condition that the parameters of Case 1 or Case 2 are satisfied, there is $\mathrm{TR}_n < \mathrm{TR}_0 < 0$ for $n \in N_0$, then if $\mathrm{DET}_n < 0$, $(n \in N_0)$, system (3) has the eigenvalue of the negative real part. Then statement (i) is proved. When the parameter relationship belongs to Case 3 and there is not $n \in N_0$ such that $\mathrm{DET}_n < 0$, then a similar method can be used to prove the conclusion. When the parameter relationship belongs to Case 3 and there is $n^1 \in N_0$ such that $\mathrm{DET}_{n^1} < 0$,then the real part of the eigenvalue $\lambda_1^{(n^1)} = (\mathrm{TR}_{n^1} + \sqrt{\mathrm{TR}_{n^1}^2 - 4\mathrm{DET}_{n^1}})/2$ of system (3) will be positive, which means that the positive equilibrium point (u_*, v_*) of system (3) becomes no longer stable. Then the statement (ii) is proved.

Next, we further analyze the necessary conditions and the boundary for the occurrence of Turing instability. Assume that

(B1) $d_2 > \varepsilon_1 d_1$ where $\varepsilon_1 = -(a_1 r + 2a_2 r)/a_1^2 + 2\sqrt{(a_1 a_2 r^2 + a_2^2 r^2)/a_1^4}$;

(B2) $d_2 > \varepsilon_2(d_1) d_1$ where $\varepsilon_2(d_1) = l^2 r/(a_1 l^2 - d_1)$

We can find that the curve $\varepsilon_2(d_1) d_1$ increases monotonically with d_1 until the first inflection point d_A, after which the curve $\varepsilon_2(d_1) d_1$ decreases linearly until the second inflection point d_B, and the value of $\varepsilon_2(d_1) d_1$ is less than zero when d_1 is greater than the second inflectiopoint d_B . (see Fig. 2(a)). To simplify the study, we only study the part of the curve $\varepsilon_2(d_1) d_1$ before the

first inflection point d_A. In this part, $\varepsilon_2(d_1)d_1$ is monotonically increasing in d_1 and intersects $\varepsilon_1 d_1$ at the point $d_1 = d_0$. We take $d_2^B(d_1) = \max_{0<d_1\leqslant d_A}\{\varepsilon_1 d_1, \varepsilon_2(d_1)d_1\}$

$$d_2^B(d_1) = \begin{cases} \varepsilon_1 d_1, & 0 < d_1 \leqslant d_0, \\ \varepsilon_2(d_1)d_1, & d_0 < d_1 \leqslant d_A. \end{cases}$$

Hence, we have the following lemma.

Lemma 1. *Suppose that* (A1) *and* (A2) *hold, then assumptions* (B1) *and* (B2) *hold if and only if* $d_2 > d_2^B(d_1), 0 < d_1 \leqslant d_A$.

Proof. Let $\varepsilon = d_2/d_1$ and $x = d_1 n^2/l^2 > 0$, then we can rewrite DET_n as $\mathrm{DET}_n = \varepsilon x^2 + (r - a_1\varepsilon)x - (a_1 + a_2)r$. Obviously, the symmetry axis is $x = (a_1\varepsilon - r)/(2\varepsilon)$, and at this time, DET_n can be taken to the minimum $(-4\varepsilon(a_1 + a_2)r - (r - a_1\varepsilon)^2)/(4\varepsilon)$.

Since $x > 0$, then $a_1\varepsilon - r > 0$. If we want $\mathrm{DET}_{n\min} < 0$ with the condition $a_1\varepsilon - r > 0$ ε must satisfy $\varepsilon > (-a_1 r - 2a_2 r)/a_1^2 + 2\sqrt{(a_1 a_2 r^2 + a_2^2 r^2)/(a_1^4)} = \varepsilon_1$ Then we can obtain $d_2 > \varepsilon_1 d_1, d_1 > 0$

When x takes a value on the axis of symmetry, n can be taken to the minimum, and we can get $n_{\min} = \sqrt{(a_1\varepsilon - r)/(2\varepsilon)\cdot(l^2/d_1)}$. To ensure that $\sqrt{(a_1\varepsilon - r)/(2\varepsilon)\cdot l^2/d_1} > \sqrt{1/2}$, then $\varepsilon > l^2 r/(a_1 l^2 - d_1) = \varepsilon_2(d_1)$ is required. Then we can gain $d_2 > \varepsilon_2(d_1)d_1$.In the part of the curve $\varepsilon_2(d_1)d_1$ before the first inflection point d_A, $\varepsilon_2(d_1)d_1$ increases monotonically with d_1 and intersects with $\varepsilon_1 d_1$ at the point $d_1 = d_0$, where $d_0 = 2a_1 l^2(-a_1 - a_2 + \sqrt{a_2(a_1 + a_2)})/(-a_1 - 2a_2 + 2\sqrt{a_2(a_1 + a_2)})$

Denote

$$d_2^n(d_1) = \frac{l^2(a_1 l^2 r + a_2 l^2 r - d_1 n^2 r)}{n^2(-a_1 l^2 + d_1 n^2)}, \quad 0 < d_1 < d_n,$$

where $d_n = (a_1 l^2 + a_2 l^2)/n^2$, then $\mathrm{DET}_n = 0$ when $d_2 = d_2^n(d_1)$. We can find that the curve $d_2^n(d_1)$ increases monotonically with d_1 until the first inflection point d_A^n, after which the curve $d_2^n(d_1)$ decreases linearly until the second inflection point d_B^n, and the value of $d_2^n(d_1)$ is less than zero when d_1 is greater than the second inflection point d_B^n (see Fig. 2(b)). For simplicity, only the part of the curve $d_2^n(d_1)$ before the first inflection point d_A^n is studied in this section. Since both d_1 and d_2 are positive parameters, this qualification makes sense.

Lemma 2. *Suppose that* (A1) *and* (A2) *hold, function* $d_2 = d_2^n(d_1), 0 < d_1 \leqslant d_A^n$ *, has the following properties*:

i. $d_2 = d_2^n(d_1)$ increases monotonically with d_1 and intersects $\varepsilon_1 d_1$ *at* $d_1 = d_M(n)$, and $d_1 = d_M(n)$ decreases monotonically as n increases, where$d_M(n) = (a_1 + a_2 + \sqrt{a_2(a_1 + a_2)})l^2/n^2$..
ii. For $n \in N$, the equation $d_2^n(d_1) = d_2^{n+1}(d_1)$ only has one root $d_{n,n+1} \in (d_M(n+1), d_M(n))$, and $d_2^n(d_1) < d_2^{n+1}(d_1) < d_2^{n+2}(d_1) < \cdots, d_1 > d_{n,n+1}$.
iii. Define $d_2 = d_2^*(d_1) = d_2^n(d_1), d_1 \in (d_{n,n+1}, d_{n-1,n}), n \in N$, then $d_2^*(d_1) \geqslant d_2^B(d_1)$. Moreover, $d_2^*(d_1) = d_2^B(d_1)$ if and only if $d_1 = d_M(n), n \in N$.

Theorem 4. *Suppose that* (A1) *and* (A2) *hold.*

i. For any given $n_1 \in N$, when $d_2 = d_2^{n_1}(d_1)$, system (3) occurs Turing bifurcation at the positive equilibrium point (u_*, v_*).

ii. $d_2 = d_2^*(d_1)$, $0 < d_1 \leqslant d_A$, is the critical curve of Turing instability

   a) If $0 < d_2 < d_2^*(d_1)$, $0 < d_1 \leqslant d_A$, system (3) is asymptotically stable at (u_*, v_*).

   b) If $d_2 > d_2^*(d_1)$, $0 < d_1 \leqslant d_A$, Turing instability occurs in system (3) at (u_*, v_*).

In Fig. 3(a), we characterize a graph of functions $d_2 = \varepsilon_1 d_1$, $d_2 = \varepsilon_2(d_1)d_1$, and $d_2 = d_2^n(d_1)$, $0 < d_1 \leqslant d_A^n$, $n = 1, 2, 3$, which will help us understand the results of Lemmas 1 and 2. In Fig. 3(b), we present a graph of the Turing bifurcation line $d_2 = d_2^*(d_1)$, $0 < d_1 \leqslant d_A$.

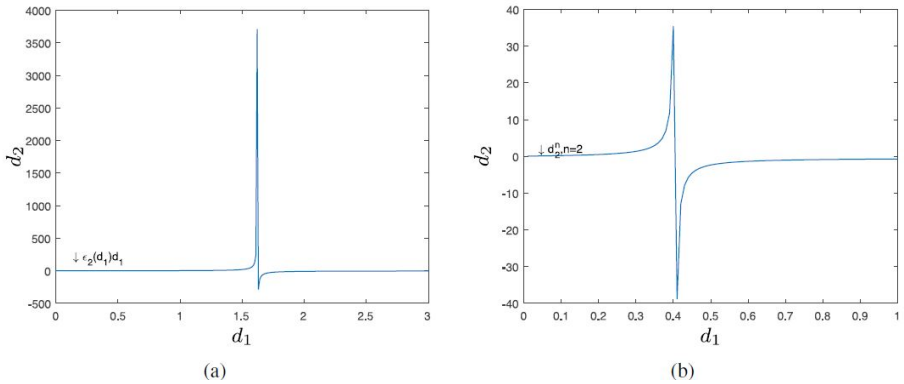

Figure 2

(a) The curve of d2 = ε2(d1)d1. (b) The curve of d2 = dn(d1) at n = 2. Keeping the other parameters fixed at the values: m = 0.35, β = 1.28, K = 0.01, l = 2.

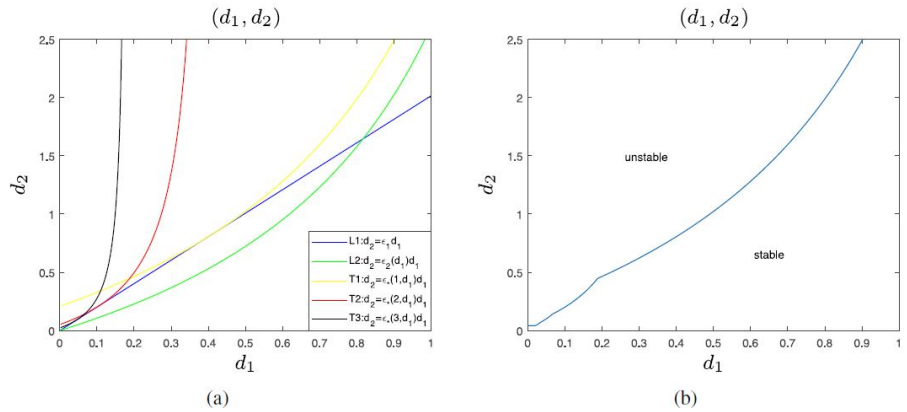

Figure 3

(a) The figure of functions d2 = ε1d1, d2 = ε2(d1)d1, and d2 = dn(d1), 0 < d1 n = 1, 2, 3 in d1, d2-plane. (b) The Turing bifurcation line d2 = d2#(d1) (0 < d1 ≤ dA). Keeping the other parameters fixed at the values: m = 0.35, β = 1.28, K = 0.01, l = 2.

3.2 Turing–Hopf bifurcation

3.2.1Hopf bifurcation and Turing–Hopf bifurcation with r and d2 as parameters

In this section, the existence conditions of the Hopf bifurcation with r as the parameter are first analyzed. Denote

$$r = r_n = -(d_1 + d_2)\mu_n + a_1, \quad n \in N_0.$$

Obviously, $\mathrm{DET}_0(r_0) = -a_1(a_1 + a_2) > 0$ under hypothesis (A2). Denote

$$\Lambda = \{n \in N_0 \mid \mathrm{DET}_n > 0 \text{ and } r_n > 0\}.$$

After analysis, we can get the following theorem.

Theorem 5. Suppose (A2) holds. System (3) undergoes a Hopf bifurcation at (u_*, v_*) when $r = r_n$, for $n \in \Lambda$. Moreover, the bifurcating periodic solution is spatially homogeneous when $r = r_0$ and spatially nonhomogeneous when $r = r_n$ for $n \in \Lambda$ and $n \neq 0$.

Proof. Let $\lambda_n(r_n) = \alpha_n(r_n) \pm i\eta_n(r_n)$, $n \in \Lambda$, be the roots of Eq. (6).

i. When $r = r_n$, we can get $\mathrm{TR}_n(r) = 0$ and $\mathrm{DET}_n(r) > 0$ for $n \in \Lambda$, then Eq. (6) has a pair of pure imaginary roots $\lambda_n(r_n) = \pm i\sqrt{\mathrm{DET}_n(r_n)}$.
ii. When r is near r_n, from Eq. (8) we can get

$$\alpha_n(r) \pm i\eta_n(r) = \frac{\mathrm{TR}_n(r) \pm \sqrt{\mathrm{TR}_n^2(r) - 4\,\mathrm{DET}_n(r)}}{2}.$$

Then we can obtain $\mathrm{d}\alpha_n(r)/\mathrm{d}r = -1/2 < 0$. That is to say, for each r_n, $n \in \Lambda$, the transversal condition holds. This completes the proof.

Next, the existence conditions of the Turing–Hopf bifurcation with r and d_2 as parameters are analyzed. System (3) will undergo a Turing–Hopf bifurcation when the following conditions are satisfied:

i. When $n = 0$, Eq. (6) has a pair of pure imaginary roots $\pm i\omega$. This phenomenon can be produced when $r = r_0 = a_1$
ii. When $n > 0$, Eq. (6) has a single zero root. This phenomenon can be produced when $\mathrm{DET}_n = 0$.

In this section, we assume (A2) always holds. Denote

$$d_2^n = r\left(\frac{d_1\mu_n - (a_1 + a_2)}{\mu_n(a_1 - d_1\mu_n)}\right), \qquad S = \{n \in N \mid a_1 - d_1\mu_n > 0\}$$

such that

$$d_2^{n_*} = r^*\left(\frac{d_1\mu_{n_*} - (a_1 + a_2)}{\mu_{n_*}(a_1 - d_1\mu_{n_*})}\right) = \min_{n\in S} r^*\left(\frac{d_1\mu_n - (a_1 + a_2)}{\mu_n(a_1 - d_1\mu_n)}\right).$$

From the Theorem 5 we can know that system (3) will have a Hopf bifurcation at the positive equilibrium point (u_*, v_*) when $r = r_0 = a_1$. Therefore, $r^* = a_1$ when $n = n_*$. d_2^n are the Turing bifurcation lines, and r^* is the Hopf bifurcation line. When$n = n_*$, we hope to find the first intersection of these two types of bifurcation lines in the first quadrant as the Turing–Hopf bifurcation point. After the above analysis, we can get the following theorem.

Theorem 6. Suppose hypothesis (A2) holds. For system (3), the following statements are correct:

i. If $S = \emptyset$, system (3) does not undergo Turing–Hopf bifurcation.
ii. If $S = \emptyset$, system (3) undergoes Turing–Hopf bifurcation at the point $(r, d_2) = (r^*, d_2^{n_*})$, and the positive equilibrium (u_*, v_*) of system (3) is locally asymptotically stable when $(r, d_2) \in Q$, where

$$Q := \left\{(r, d_2) \;\middle|\; r > r^*,\ 0 < d_2 < r\left(\frac{d_1\mu_{n_*} - (a_1 + a_2)}{\mu_{n_*}(a_1 - d_1\mu_{n_*})}\right)\right\}.$$

Proof. In r, d_2-plane, the Turing bifurcation curves are

$$\mathcal{L}_n\colon\ d_2^n = r\left(\frac{d_1\mu_n - (a_1 + a_2)}{\mu_n(a_1 - d_1\mu_n)}\right), \quad n \in S.$$

The Hopf bifurcation curve is $\mathcal{H}_0\colon\ r = r^*$.

i. If $S = \emptyset$, then there is no intersection point between Turing bifurcation curves $\mathcal{L}_n$ and the Hopf bifurcation curve $\mathcal{H}_0$ in the first quadrant. This indicates that system (3) does not undergo Turing–Hopf bifurcation.
ii. If $S = \emptyset$, then the Turing bifurcation curve $\mathcal{L}_{n_*}$ and the Hopf bifurcation curve $\mathcal{H}_0$ intersect at point $(r^*, d_2^{n_*})$. This point is called the Turing–Hopf bifurcation point. In addition, when$(r, d_2) \in Q$, it is easy to prove that $\mathrm{TR}_n < 0$ and $\mathrm{DET}_n > 0$ for $n \in N_0$. Then the positive equilibrium point (u_*, v_*) is locally asymptotically stable. Next, let us verify the transversality conditions. Suppose $\lambda_1(r, d_2) = \alpha_1(r, d_2) + \mathrm{i}\eta_1(r, d_2)$ with $\alpha_1(r^*) = 0, \eta_1(r^*) = \omega > 0$ when $n = 0$, and $\lambda_2(r, d_2) = \alpha_2(r, d_2) + \mathrm{i}\eta_2(r, d_2)$ with $\alpha_2(r^*, d_2^{n_*}) = 0, \eta_2(r^*, d_2^{n_*}) = 0$ when $n = n_* > 0$, then the transversality conditions are as follows:

$$\left.\frac{\mathrm{d}\,\mathrm{Re}(\lambda_1(r,d_2))}{\mathrm{d}r}\right|_{r=a_1,\mathcal{H}_0} = -\frac{1}{2} < 0,$$

$$\left.\frac{\mathrm{d}\,\mathrm{Re}(\lambda_2(r,d_2))}{\mathrm{d}r}\right|_{r=a_1,\mathcal{L}_{n_*}} = \frac{d_1\mu_{n_*} - (a_1+a_2)}{\mathrm{TR}_{n_*}} < 0.$$

This completes the proof.

3.2.2 Hopf bifurcation and Turing–Hopf bifurcation with K and d2 as parameters

In this section, the existence conditions of the Hopf bifurcation with K as the parameter are first analyzed. Denote

$$K = K_n = \frac{K_A}{K_B}, \quad n \in N_0,$$

where

$$K_A = (1+m)^2\left[(1+r)\left(1+2m+m^2\right) - 2\beta + (d_1+d_2)(1+m)^2\mu_n\right]$$

and

$$\begin{aligned} K_B = {} & (1+m)^4 r^2 + (-3+m)(1+m)^2 r\beta - 2(-1+m)\beta^2 \\ & + (d_1+d_2)(1+m)^2\left(2(1+m)^2 r + (-3+m)\beta\right)\mu_n \\ & + (d_1+d_2)^2(1+m)^4\mu_n^2. \end{aligned}$$

Obviously, $\mathrm{DET}_0(K_0) = -r(a_1+a_2) > 0$ under hypothesis (A2). Denote $\Lambda' = \{n \in N_0 \mid \mathrm{DET}_n > 0 \text{ and } K_n > 0\}$. Then we make the following hypotheses:

(C1) $1 + m - K\beta > 0$;

(C2) $2 + 4m + 2m^2 + K\beta^2 \neq \beta + m\beta + \beta\sqrt{C}$, where $C = -4(K+Km) \times (-1-m+\beta) + (1+m+K\beta)^2$.

After analysis, we can get the following theorem.

Theorem 7. Suppose (A2), (C1) and (C2) hold. System (3) undergoes a Hopf bifurcation at (u_*, v_*) when $K = K_n$ for $n \in \Lambda$.. Moreover, the bifurcating periodic solution is spatially homogeneous when $K = K_n > 0$ and spatially nonhomogeneous when $K = K_n$ for $n \in \Lambda.'$ and $n \neq 0$..

Next, the existence conditions of the Turing–Hopf bifurcation with K and d_2 as parameters are analyzed. In this section, we assume (A2) always holds. Denote

$$d_2^n = r\left(\frac{d_1\mu_n - (a_1+a_2)}{\mu_n(a_1 - d_1\mu_n)}\right), \qquad S = \{n \in N \mid a_1 - d_1\mu_n > 0\}$$

such that

$$d_2^{n_*} = r\left(\frac{d_1\mu_{n_*} - (a_1+a_2)}{\mu_{n_*}(a_1 - d_1\mu_{n_*})}\right)\Big|_{K=K_0} = \min_{n\in S} r\left(\frac{d_1\mu_n - (a_1+a_2)}{\mu_n(a_1 - d_1\mu_n)}\right)\Big|_{K=K_0}.$$

From Theorem 7 we can know that system (3) will have a Hopf bifurcation at (u_*, v_*) when $K = K_0$. Therefore, $K = K_0$ when $n = n_*$. d_2^n are the Turing bifurcation lines, and K_0 is the Hopf bifurcation line. When $n = n_*$., we hope to find the first intersection of these two types of bifurcation lines in the first quadrant as the Turing–Hopf bifurcation point. After the above analysis, we can get the following theorem.

Theorem 8. Suppose hypothesis (A2), (C1), and (C2) hold. For system (3), the following statements are correct:

i. If $S = \emptyset$, system (3) does not undergo Turing–Hopf bifurcation.
ii. If $S = \emptyset$, system (3) undergoes Turing–Hopf bifurcation at the point $(K, d_2) = (K_0, d_2^{n_*})$

The proofs of Theorems 7 and 8 are similar to those of Theorems 5 and 6, respectively, and will not be repeated here

4 Normal forms for Turing–Hopf bifurcation with r and *d2* as parameters

In this section, we calculate the normal forms of the Turing–Hopf bifurcation for the reaction–diffusion system (3) at the coexistence equilibrium (u_*, v_*). Firstly, we introduce the parameters σ_1 and σ_2 by letting $r = r^* + \sigma_1$ and $d_2 = d_2^{n_*} + \sigma_2$, which satisfy that the reaction–diffusion system (3) will undergo Turing–Hopf bifurcation at the positive equilibrium point (u_*, v_*) when $\sigma_1 = 0$ and $\sigma_2 = 0$. Then system (3) can be transformed into

$$\begin{aligned}\frac{\partial u}{\partial t} &= d_1\Delta u + \frac{u}{1+Kv} - u^2 - \frac{\beta u^2 v}{u^2 + mv^2},\\ \frac{\partial v}{\partial t} &= (d_2^{n_*} + \sigma_2)\Delta v + (r^* + \sigma_1)v\left(1 - \frac{v}{u}\right).\end{aligned} \tag{9}$$

For system (9), (u_*, v_*) is still the positive equilibrium point. Let us make the transformations $\bar{u} = u - u_*$ and $\bar{v} = v - v_*$ to move (u_*, v_*) to the origin. After omitting the horizontal bar, system (9) becomes

$$\begin{aligned}\frac{\partial u}{\partial t} &= d_1\Delta u + \frac{u+u_*}{1+K(v+v_*)} - (u+u_*)^2 - \frac{\beta(u+u_*)^2(v+v_*)}{(u+u_*)^2 + m(v+v_*)^2},\\ \frac{\partial v}{\partial t} &= (d_2^{n_*} + \sigma_2)\Delta v + (r^* + \sigma_1)(v+v_*)\left(1 - \frac{v+v_*}{u+u_*}\right).\end{aligned} \tag{10}$$

Then according to [7], for system (10), we can get

$$D(\sigma)=\begin{pmatrix} d_1 & 0 \\ 0 & d_2^{n_*}+\sigma_2 \end{pmatrix}, \qquad L(\sigma)=\begin{pmatrix} r^* & a_2 \\ r^*+\sigma_1 & -(r^*+\sigma_1) \end{pmatrix},$$
$$F(\phi,\sigma)=\begin{pmatrix} \frac{\phi_1+u_*}{1+K(\phi_2+v_*)}-(\phi_1+u_*)^2-\frac{\beta(\phi_1+u_*)^2(\phi_2+v_*)}{(\phi_1+u_*)^2+m(\phi_2+v_*)^2}-r^*\phi_1-a_2\phi_2 \\ (r^*+\sigma_1)(\phi_2+v_*)(1-\frac{\phi_2+v_*}{\phi_1+u_*})-(r^*+\sigma_1)\phi_1+(r^*+\sigma_1)\phi_2 \end{pmatrix},$$

where $\phi=(\phi_1,\phi_2)^{\mathrm{T}}\in X$. Then we can obtain

$$D(0)=\begin{pmatrix} d_1 & 0 \\ 0 & d_2^{n_*} \end{pmatrix}, \qquad D_1(\sigma)=\begin{pmatrix} 0 & 0 \\ 0 & 2\sigma_2 \end{pmatrix},$$
$$L(0)=\begin{pmatrix} r^* & a_2 \\ r^* & -r^* \end{pmatrix}, \qquad L_1(\sigma)=\begin{pmatrix} 0 & 0 \\ 2\sigma_1 & -2\sigma_1 \end{pmatrix},$$
$$Q(\phi,\psi)=\begin{pmatrix} \alpha_{11}\phi_1\psi_1+\alpha_{12}(\phi_1\psi_2+\psi_1\phi_2)+\alpha_{13}\phi_2\psi_2 \\ \alpha_{21}\phi_1\psi_1+\alpha_{22}(\phi_1\psi_2+\psi_1\phi_2)+\alpha_{23}\phi_2\psi_2 \end{pmatrix},$$
$$C(\phi,\psi,\upsilon)=\begin{pmatrix} \beta_{11}\phi_1\psi_1\upsilon_1+\beta_{12}(\phi_1\psi_1\upsilon_2+\phi_1\psi_2\upsilon_1+\phi_2\psi_1\upsilon_1) \\ \quad +\beta_{13}(\phi_1\psi_2\upsilon_2+\phi_2\psi_1\upsilon_2+\phi_2\psi_2\upsilon_1)+\beta_{14}\phi_2\psi_2\upsilon_2 \\ \beta_{21}\phi_1\psi_1\upsilon_1+\beta_{22}(\phi_1\psi_1\upsilon_2+\phi_1\psi_2\upsilon_1+\phi_2\psi_1\upsilon_1) \\ \quad +\beta_{23}(\phi_1\psi_2\upsilon_2+\phi_2\psi_1\upsilon_2+\phi_2\psi_2\upsilon_1)+\beta_{24}\phi_2\psi_2\upsilon_2 \end{pmatrix}$$

with

$$\alpha_{11}=-2-\frac{2(-3+m)m\beta}{(1+m)^3u_*}, \qquad \alpha_{12}=-\frac{K}{(1+Ku_*)^2}+\frac{2(-3+m)m\beta}{(1+m)^3u_*},$$
$$\alpha_{13}=\frac{2K^2u_*}{(1+Ku_*)^3}-\frac{2(-3+m)m\beta}{(1+m)^3u_*}, \quad \alpha_{21}=-\frac{2r^*}{u_*}, \quad \alpha_{22}=\frac{2r^*}{u_*}, \quad \alpha_{23}=-\frac{2r^*}{u_*},$$

$$\beta_{11}=\frac{24(-1+m)m\beta}{(1+m)^4u_*^2}, \qquad \beta_{12}=\frac{2m(9-14m+m^2)\beta}{(1+m)^4u_*^2},$$
$$\beta_{13}=\frac{2K^2}{(1+Ku_*)^3}-\frac{4m(3-8m+m^2)\beta}{(1+m)^4u_*^2},$$
$$\beta_{14}=-\frac{6K^3u_*}{(1+Ku_*)^4}+\frac{6m(1-6m+m^2)\beta}{(1+m)^4u_*^2},$$
$$\beta_{21}=\frac{6r^*}{u_*^2}, \qquad \beta_{22}=-\frac{4r^*}{u_*^2}, \qquad \beta_{23}=\frac{2r^*}{u_*^2}, \qquad \beta_{24}=0,$$

and $\phi=(\phi_1,\phi_2)^{\mathrm{T}}, \psi=(\psi_1,\psi_2)^{\mathrm{T}}, \upsilon=(\upsilon_1,\upsilon_2)^{\mathrm{T}}\in X$.

The characteristic matrix corresponding to system (10) is

$$D_n(\lambda)=\begin{pmatrix} \lambda-r^*+d_1\mu_n & -a_2 \\ -r^* & \lambda+r^*+d_2^{n_*}\mu_n \end{pmatrix}, \quad n\in N.$$

According to Theorem 6, $\lambda=\pm i\omega$ with $\omega=\sqrt{-r^*(a_1+a_2)}$ are eigenvalues of $D_0(\lambda)$, and $\lambda=0$ is a simple eigenvalue for $D_{n_*}(\lambda)$ with other eigenvalues having negative real parts. Then, by straightforward calculations, we have

$$\phi_1 = \begin{pmatrix} 1 \\ \frac{d_1\mu_{n_*} - r^*}{a_2} \end{pmatrix}, \qquad \psi_1 = \begin{pmatrix} \frac{a_2 r^*}{(d_1\mu_{n_*} - r^*)^2 + a_2 r^*} \\ \frac{a_2(d_1\mu_{n_*} - r^*)}{(d_1\mu_{n_*} - r^*)^2 + a_2 r^*} \end{pmatrix}^{\mathrm{T}},$$

$$\phi_2 = \begin{pmatrix} 1 \\ \frac{\mathrm{i}\omega - r^*}{a_2} \end{pmatrix}, \qquad \psi_2 = \begin{pmatrix} \frac{a_2 r^*}{(i\omega - r^*)^2 + a_2 r^*} \\ \frac{a_2(i\omega - r^*)}{(i\omega - r^*)^2 + a_2 r^*} \end{pmatrix}^{\mathrm{T}}.$$

Therefore, $\Phi = (\phi_1, \phi_2, \bar{\phi}_2)$ and $\Psi = (\psi_1, \psi_2, \bar{\psi}_2)^{\mathrm{T}}$. satisfying $\Phi\Psi = I_3$, where I_3 is the identity matrix. By [7], we can compute the following parameters:

$$\begin{aligned}
a_1(\sigma) &= \frac{1}{2}\psi_1(L_1(\sigma)\phi_1 - \mu_{n_*} D_1(\sigma)\phi_1), \qquad a_{200} = a_{011} = b_{110} = 0,\\
b_2(\sigma) &= \frac{1}{2}\psi_2\big(L_1(\sigma)\phi_2 - 0D_1(\sigma)\phi_2\big),\\
a_{300} &= \frac{1}{4}\psi_1 C_{\phi_1\phi_1\phi_1} + \frac{1}{\omega}\psi_1 \operatorname{Re}[\mathrm{i}Q_{\phi_1\phi_2}\psi_2]Q_{\phi_1\phi_1} + \psi_1 Q_{\phi_1(h^0_{200} + h^{2n_*}_{200}/\sqrt{2})},\\
a_{111} &= \psi_1 C_{\phi_1\phi_2\bar{\phi}_2} + \frac{2}{\omega}\psi_1 \operatorname{Re}[\mathrm{i}Q_{\phi_1\phi_2}\psi_2]Q_{\phi_2\bar{\phi}_2} + \psi_1(Q_{\phi_1(h^0_{011} + h^{2n_*}_{011}/\sqrt{2})}\\
&\quad + Q_{\phi_2 h^{n_*}_{101}} + Q_{\bar{\phi}_2 h^{n_*}_{110}}),\\
b_{210} &= \frac{1}{2}\psi_2 C_{\phi_1\phi_1\phi_2} + \frac{1}{2\mathrm{i}\omega}\psi_2\big(2Q_{\phi_1\phi_1}\psi_1 Q_{\phi_1\phi_2} + (-Q_{\phi_2\phi_2}\psi_2 + Q_{\phi_2\bar{\phi}_2}\bar{\psi}_2)Q_{\phi_1\phi_1}\big)\\
&\quad + \psi_2(Q_{\phi_1 h^{n_*}_{110}} + Q_{\phi_2 h^0_{200}}),\\
b_{021} &= \frac{1}{2}\psi_2 C_{\phi_2\phi_2\bar{\phi}_2} + \frac{1}{4\mathrm{i}\omega}\psi_2\left(\frac{2}{3}Q_{\bar{\phi}_2\bar{\phi}_2}\bar{\psi}_2 Q_{\phi_2\phi_2} + (-2Q_{\phi_2\phi_2}\psi_2 + 4Q_{\phi_2\bar{\phi}_2}\bar{\psi}_2)Q_{\phi_2\bar{\phi}_2}\right)\\
&\quad + \psi_2(Q_{\phi_2 h^0_{011}} + Q_{\bar{\phi}_2 h^0_{020}}),
\end{aligned}$$

where

$$\begin{aligned}
h^0_{200} &= -\frac{1}{2}L^{-1}(0)Q_{\phi_1\phi_1} + \frac{1}{2\omega i}(\phi_2\psi_2 - \bar{\phi}_2\bar{\psi}_2)Q_{\phi_1\phi_1},\\
h^{2n_*}_{200} &= -\frac{1}{2\sqrt{2}}[L(0) - 4\mu_{n_*}D(0)]^{-1}Q_{\phi_1\phi_1},\\
h^0_{011} &= -L^{-1}(0)Q_{\phi_2\bar{\phi}_2} + \frac{1}{\omega i}(\phi_2\psi_2 - \bar{\phi}_2\bar{\psi}_2)Q_{\phi_2\bar{\phi}_2},\\
h^0_{020} &= \frac{1}{2}[2i\omega I - L(0)]^{-1}Q_{\phi_2\phi_2} - \frac{1}{2\omega i}\left(\phi_2\psi_2 + \frac{1}{3}\bar{\phi}_2\bar{\psi}_2\right)Q_{\phi_2\phi_2},\\
h^{n_*}_{110} &= \big[\mathrm{i}\omega I - \big(L(0) - \operatorname{diag}(-\mu_{n_*}, -d_{n_*}\mu_{n_*})\big)\big]^{-1}Q_{\phi_1\phi_2} - \frac{1}{\omega\mathrm{i}}\phi_1\psi_1 Q_{\phi_1\phi_2},\\
h^0_{002} &= \overline{h^0_{020}}, \qquad h^{n_*}_{101} = \overline{h^{n_*}_{110}}, \qquad h^{2n_*}_{011} = 0.
\end{aligned}$$

According to [7], the normal form restricted to the third order on the central manifold of the reaction–diffusion system (3) at the Turing–Hopf singularity is

$$\begin{aligned}
\dot{z_1} &= a_1(\sigma)z_1 + a_{200}z_1^2 + a_{011}z_2\bar{z}_2 + a_{300}z_1^3 + a_{111}z_1z_2\bar{z}_2 + \text{h.o.t.},\\
\dot{z_2} &= \mathrm{i}\omega z_2 + b_2(\sigma)z_2 + b_{110}z_1z_2 + b_{210}z_1^2z_2 + b_{021}z_2^2\bar{z}_2 + \text{h.o.t.},\\
\dot{\bar{z}_2} &= -\mathrm{i}\omega\bar{z}_2 + \bar{b}_2(\sigma)\bar{z}_2 + \bar{b}_{110}z_1\bar{z}_2 + \bar{b}_{210}z_1^2\bar{z}_2 + \bar{b}_{021}z_2\bar{z}_2{}^2 + \text{h.o.t.}
\end{aligned} \tag{11}$$

Through the parameter transformation $z_1 = r$, $z_2 = \rho\cos\theta - \mathrm{i}\rho\sin\theta$, the normal form equation (11) can be rewritten into real coordinates form (the third-order term is truncated, and the azimuth angle is removed item θ)

$$\begin{aligned}\dot{r} &= a_1(\sigma)r + a_{300}r^3 + a_{111}r\rho^2,\\ \dot{\rho} &= \mathrm{Re}\big(b_2(\sigma)\big)\rho + \mathrm{Re}(b_{210})\rho r^2 + \mathrm{Re}(b_{021})\rho^3.\end{aligned}$$

5 Numerical simulations

5.1 Numerical simulations of Turing–Hopf bifurcation with r and d2 as parameters

In this section, we perform the numerical simulations. Taking $m = 0.35$, $\beta = 1.28$ $d_1 = 0.02$, $K = 0.01$, $l = 1$, we have

$$\begin{aligned}\frac{\partial u}{\partial t} &= 0.02\Delta u + \frac{u}{1+0.01v} - u^2 - \frac{1.28u^2v}{u^2+0.35v^2},\\ \frac{\partial v}{\partial t} &= d_2\Delta v + rv\left(1-\frac{v}{u}\right).\end{aligned} \tag{12}$$

Through calculation, we get the unique positive equilibrium point $(u_*, v_*) \approx (0.0513, 0.0513)$. $a_1 \approx 0.4052$, $a_2 \approx -0.4570$. then hypothesis (A2) holds. In addition, $S = \{1,2,3,4\}$, $r^* \approx 0.4052$, $n_* = 2$, $d_2^{n_*} \approx 0.0411$. $\mathcal{H}_0$: $r = r^* \approx 0.4052$ is the Hopf bifurcation curve in r, d_2 -plane.

$$\mathcal{L}_n\colon\ d_2^n = r\left(\frac{d_1\mu_n - (a_1+a_2)}{\mu_n(a_1 - d_1\mu_n)}\right), \quad n \in S,$$

are the Turing bifurcation curves. Then the normal form restricted on center manifold for the reaction–diffusion system (12) at Turing–Hopf singularity is

$$\begin{aligned}\dot{z_1} &= (-0.5397\sigma_1 + 5.3245\sigma_2)z_1 - 88.1722z_1^3 - 56.7982z_1z_2\bar{z_2} + \text{h.o.t.},\\ \dot{z_2} &= 0.1449\mathrm{i}z_2 + (-0.5000 + 0.1789\mathrm{i})\sigma_1 z_2 + (50.4645 - 1.9071\mathrm{i})z_1^2z_2\\ &\quad - (22.5514 + 1.6995\mathrm{i})z_2^2\bar{z_2} + \text{h.o.t.},\\ \dot{\bar{z}_2} &= -0.1449\mathrm{i}\bar{z_2} + (-0.5000 - 0.1789\mathrm{i})\sigma_1\bar{z}_2 + (50.4645 + 1.9071\mathrm{i})z_1^2\bar{z}_2\\ &\quad - (22.5514 - 1.6995\mathrm{i})z_2\bar{z_2}^2 + \text{h.o.t.}\end{aligned}$$

Then we have

$$\begin{aligned}\dot{r} &= (-0.5397\sigma_1 + 5.3245\sigma_2)r - 88.1722r^3 - 56.7982r\rho^2,\\ \dot{\rho} &= -0.5000\sigma_1\rho + 50.4645\rho r^2 - 22.5514\rho^3.\end{aligned} \tag{13}$$

Considering $\rho > 0$, system (13) has equilibria

$$\begin{aligned}&A_0 = (0,0),\\ &A_1^{\pm} = (\pm\sqrt{-0.0061\sigma_1 + 0.0604\sigma_2}, 0) \quad \text{for } -0.0061\sigma_1 + 0.0604\sigma_2 > 0,\\ &A_2 = (0, \sqrt{-0.0222\sigma_1}) \quad \text{for } \sigma_1 < 0,\\ &A_3^{\pm} = (\pm\sqrt{0.0033\sigma_1 + 0.0247\sigma_2}, \sqrt{-0.0147\sigma_1 + 0.0553\sigma_2})\\ &\quad \text{for } 0.0033\sigma_1 + 0.0247\sigma_2 > 0 \text{ and } -0.0147\sigma_1 + 0.0553\sigma_2 > 0.\end{aligned}$$

By [7], we know: A_0 is the coexistence equilibrium; $A_1^{\pm}$ are spatially inhomogeneous steady states; A_2 is spatially homogeneous periodic solution; $A_3^{\pm}$ are spatially inhomogeneous periodic solutions.

Then the following critical bifurcation curves can be obtained:

$$\begin{aligned}&\mathcal{H}_0\colon\ \sigma_1 = 0, \qquad \mathcal{T}\colon\ \sigma_2 = 0.1014\sigma_1,\\ &\mathcal{T}_1\colon\ \sigma_2 = -0.1351\sigma_1, \quad \sigma_1 \leqslant 0,\\ &\mathcal{T}_2\colon\ \sigma_2 = 0.2654\sigma_1, \qquad \sigma_1 \geqslant 0.\end{aligned}$$

From Fig. 4 it can be seen that the first intersection of the Turing curves $\mathcal{L}_n$ and the Hopf curve $\mathcal{H}_0$ with $(r, d_2) = (r^*, d_2^{n*})$ is chosen as the Turing–Hopf bifurcation point. Therefore, system (12) undergoes Turing–Hopf bifurcation at the point (r^*, d_2^{n*})=(0.4052,0.0411). Then the parameter plane partition diagram and phase diagram can be obtained as shown in Fig. 5.

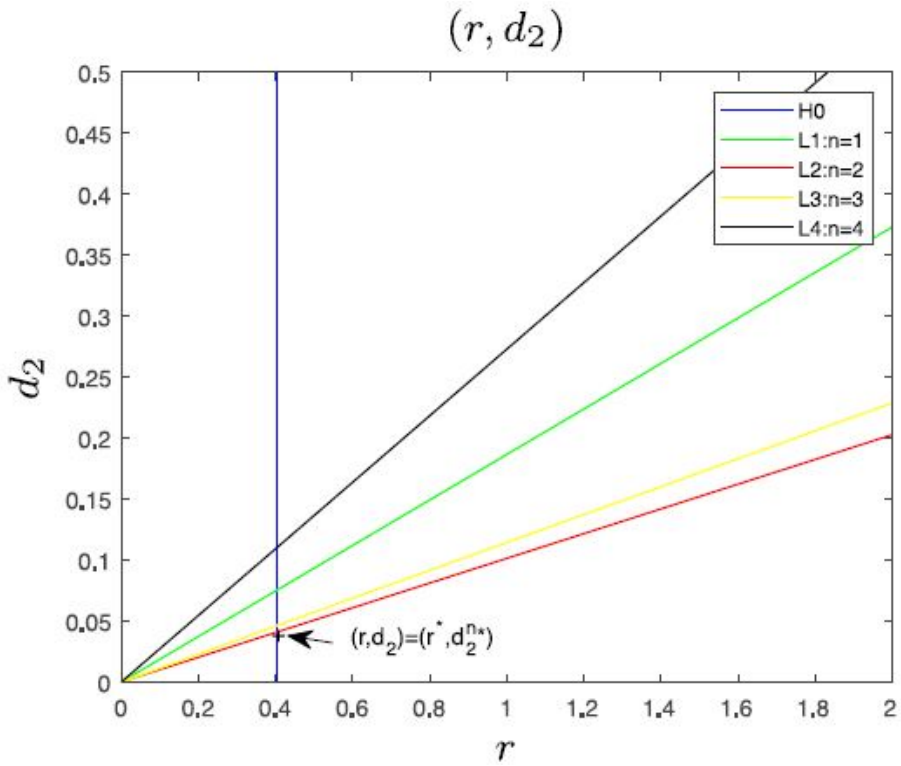

Figure 4
Turing–Hopf bifurcation point (r#, dn#) in r, d2-plane.

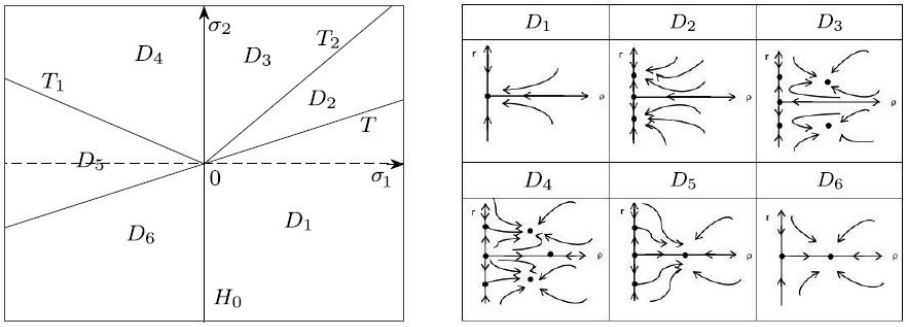

Figure 5
The bifurcation set (a) and the phase portraits (b) for Turing–Hopf bifurcation of system (12).

Proposition 1. *For given* $m = 0.35$, $\beta = 1.28$, $d_1 = 0.02$, $K = 0.01$, $l = 1$, *the plane of parameters* σ_1 , σ_2 *is divided into six regions by bifurcation curves* $\mathcal{H}_0, \mathcal{T}, \mathcal{T}_1$. *. For each region, different dynamic phenomenon are generated by system* (3). *When* $(\sigma_1, \sigma_2) \in D_1$, *system* (3) *has a locally asymptotically stable positive equilibrium point* (u_*, v_*) (*see Fig.* 6). *Conversely, when* $(\sigma_1, \sigma_2) \in D_1$, *the positive equilibrium point* (u_*, v_*) *becomes unstable. When* $(\sigma_1, \sigma_2) \in D_2$, *system* (3) *has a pair of stable spatially inhomogeneous steady states (see Fig.* 7). *The spatial patterns and bistability are shown by system* (3). *When* $(\sigma_1, \sigma_2) \in D_3$, *there are a pair of stable spatially inhomogeneous periodic solutions and a pair of unstable spatially inhomogeneous steady states (see Fig.* 8). *When* $(\sigma_1, \sigma_2) \in D_4$, *there are a pair of stable spatially inhomogeneous periodic solutions, a pair of*

unstable spatially inhomogeneous steady states, and an unstable spatially homogeneous periodic solution (see F igs. 9 and 10). *When* $(\sigma_1, \sigma_2) \in D_5$ *, there are a stable spatially homogeneous periodic solution and a pair of unstable spatially inhomogeneous steady states. There are heteroclinic solutions connecting the unstable spatially inhomogeneous steady state to stable spatially homogeneous periodic solution (see F ig.* 11). *When* $(\sigma_1, \sigma_2) \in D_6$ *, system* (3) *has a stable spatially homogeneous periodic solution (see Fig.* 12).

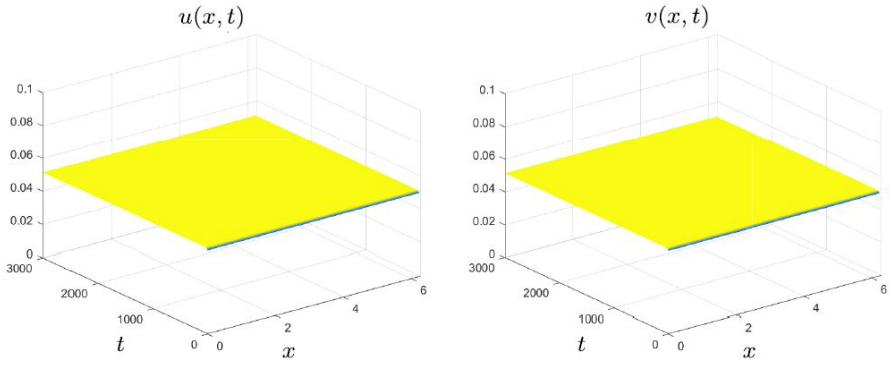

Figure 6

When (σ1, σ2) = (1, 0) lies in region D1, the positive constant equilibrium (u#, v#) = (0.0513, 0.0513) is asymptotically stable. The initial value is u(x, 0) = 0.05, v(x, 0) = 0.05.

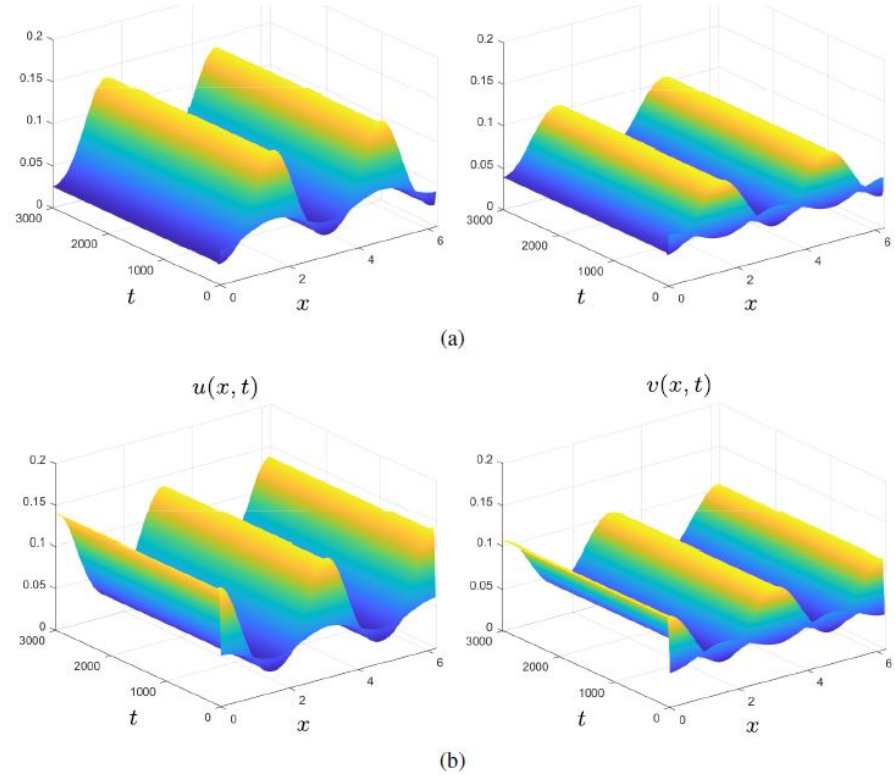

Figure 7

When (σ1, σ2) = (1, 0.2) lies in region D2, the positive constant equilibrium (u#, v#) = (0.0513, 0.0513) is unstable, and there are two stable spatially inhomogeneous steady states like cos(2x). (a) The initial value is u(x, 0) = 0.051338728 − 0.01 cos(2x), v(x, 0) = 0.051338728 + 0.01 cos(2x); (b) the initial value is u(x, 0) = 0.051338728 + 0.01 cos(2x), v(x, 0) = 0.051338728 − 0.01 cos(2x).

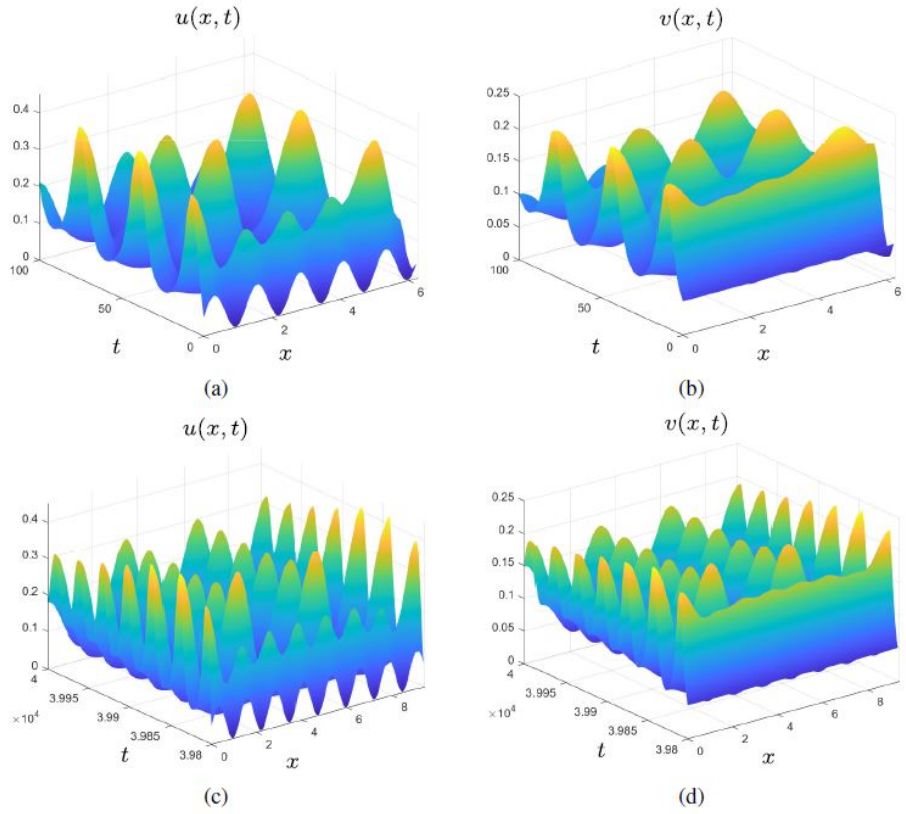

Figure 8

When (σ1, σ2) = (0.1, 0.1) lies in region D3, the positive constant equilibrium (u#, v#) = (0.0513, 0.0513) is unstable, and there are stable spatially inhomogeneous periodic solutions. The initial value is u(x, 0) = 0.051338728 + 0.05 sin(5x), v(x, 0) = 0.051338728. (a) and (b) are transient behaviours for u and v, respectively; (c) and (d) are long-term behaviours for u and v, respectively.

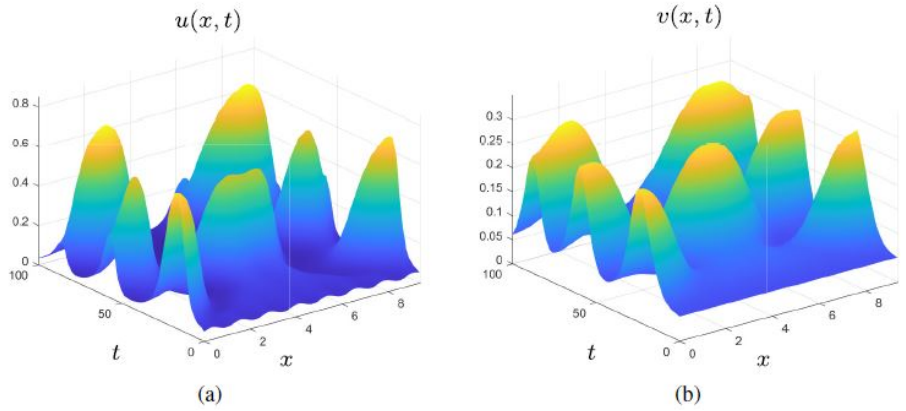

Figure 9

When (σ1, σ2) = (0.1, 0.2) lies in region D4, the positive constant equilibrium (u#, v#) = (0.0513, 0.0513) is unstable, and there are stable spatially inhomogeneous periodic solutions. The initial value is u(x, 0) = 0.051338728 + 0.01 sin(5x), v(x, 0) = 0.051338728. (a) and (b) are transient behaviours for u and v, respectively.

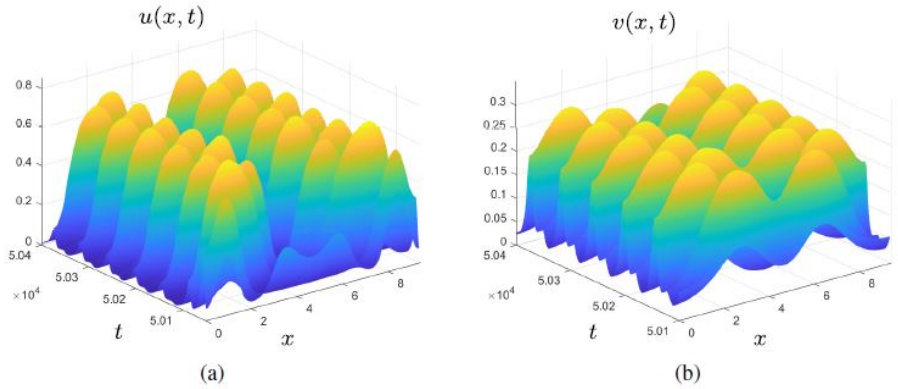

Figure 10

When (σ1, σ2) = (0.1, 0.2) lies in region D4, the positive constant equilibrium (u#, v#) = (0.0513, 0.0513) is unstable, and there are stable spatially inhomogeneous periodic solutions. The initial value is u(x, 0) = 0.051338728 + 0.01 sin(5x), v(x, 0) = 0.051338728. (a) and (b) are long-term behaviours for u and v, respectively.

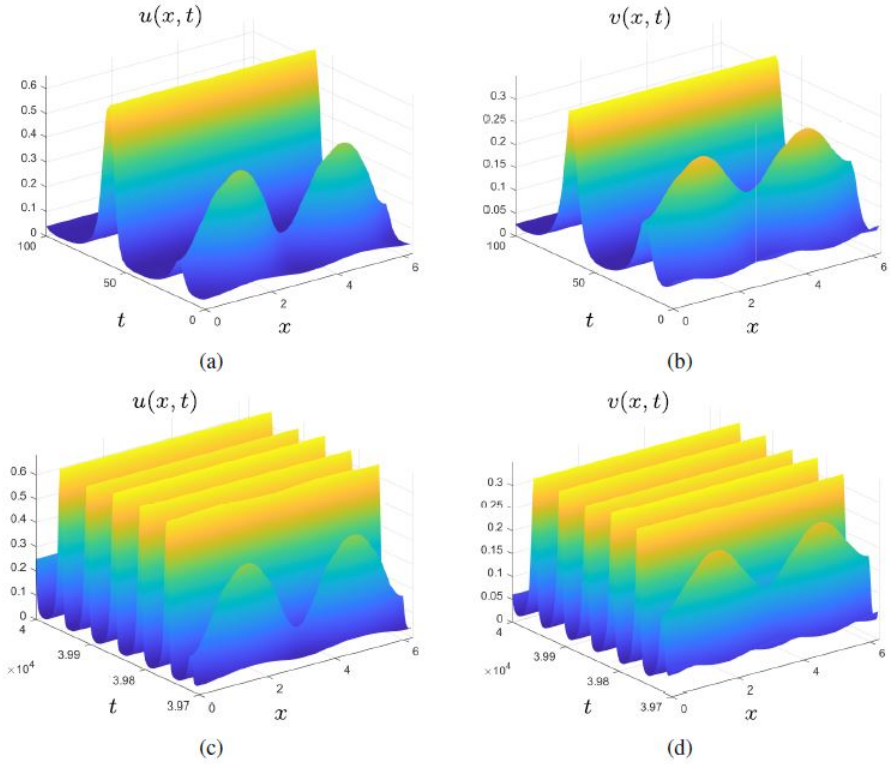

Figure 11

When (σ1, σ2) = (0.1, 0) lies in region D5, the positive constant equilibrium (u#, v#) = (0.0513, 0.0513) is unstable, and there are heteroclinic solutions connecting the unstable spatially inhomogeneous steady state to stable spatially homogeneous periodic solution. The initial value is u(x, 0) = 0.051338728 0.01 cos(2x), v(x, 0) = 0.051338728 + 0.01 cos(2x). (a) and (b) are transient behaviours for u and v, respectively; (c) and (d) are long-term behaviours for u and v, respectively.

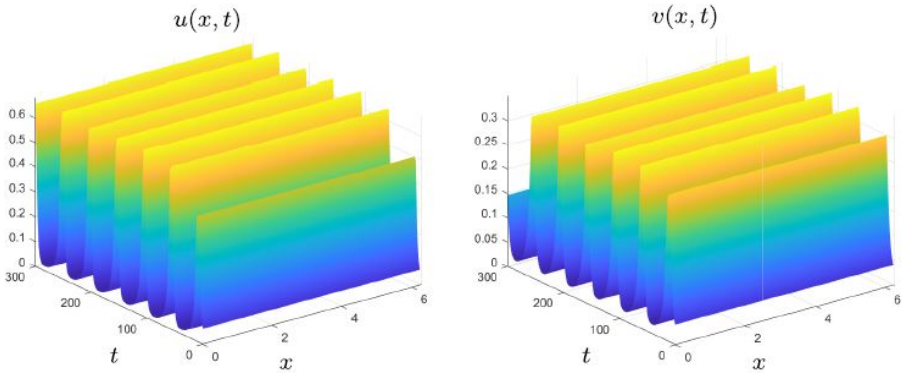

Figure 12

When (σ1, σ2) = (0.1, 0.03) lies in region D6, the positive constant equilibrium (u#, v#) = (0.0513, 0.0513) is unstable, and there is a stable spatially homogeneous periodic solution. The initial value is u(x, 0) = 0.051338728 + 0.01, v(x, 0) = 0.051338728 − 0.01.

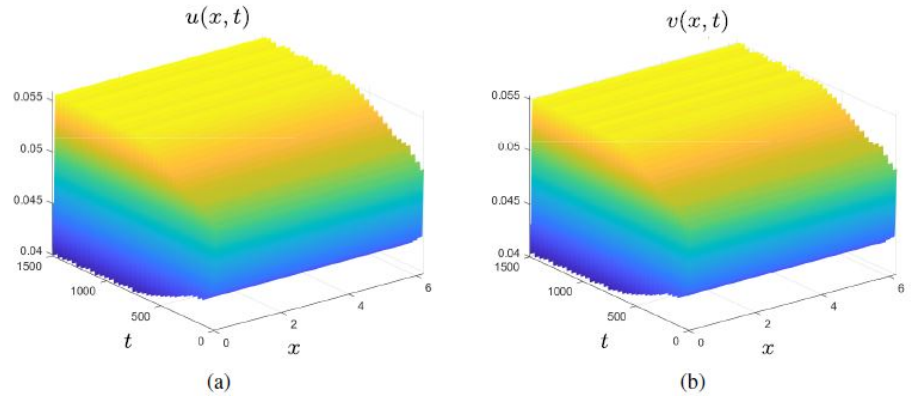

Figure 13

The numerical simulations of system (3) with K = 0.1153 and the initial condition at (0.05, 0.05).

5.2 Numerical simulations of Hopf bifurcation with K as the parameter

In this section, we perform the numerical simulations of Hopf bifurcation with K as the parameter. Taking $m = 0.35,\ \beta = 1.28,\ r = 0.41,\ d_1 = 0.02,\ d_2 = 0.0411$, we have $K = K_0 \approx 0.1153$. Through calculation, we get the unique positive equilibrium point $(u_*, v_*) \approx (0.0465, 0.0465)$. $a_1 = 0.4100,\ a_2 \approx -0.4618$, then hypothesis (A2), (C1), and (C2) hold. Figure 13 shows the numerical simulations of system (3) with Hopf bifurcation.

6 Conclusions

In this paper, we have formulated a Leslie–Gower-type predator–prey system with the fear effect and ratio-dependent Holling III functional response to consider the cost of fear on prey demography. The main focus of this study is to investigate the influence of antipredator behaviour due to fear of predators analytically and numerically. We obtain many interesting results. Mathematically, we analyze the existence and stability of the positive equilibria of the model and give conditions for the

existence of the Turing instability, the Hopf bifurcation, and the Turing–Hopf bifurcation by selecting d_2, r and K as the bifurcating parameters, respectively. In addition, we calculate the normal form of system (3) and divide the plane of parameters σ_1, σ_2 into six regions D_1–D_6. In each region, we demonstrate that the predator–prey model exhibits complex spatiotemporal dynamics including spatially homogeneous periodic solutions, spatially inhomogeneous periodic solutions, and spatially inhomogeneous steady-state solutions. Ecologically, we show that if the model has a unique positive equilibrium, the fear effect can reduce the density of predator and prey: as the level of fear K increases, both the predator and prey density gradually decrease. Moreover, depending on the predator and prey's different states in each region, we can give solutions accordingly.

Acknowledgments

The authors wish to express their gratitude to the editors and the reviewers for the helpful comments.

References

1. X. Cao, W. Jiang, Turing–Hopf bifurcation and spatiotemporal patterns in a diffusive predator– prey system with Crowley–Martin functional response, *Nonlinear Anal., Real World Appl.*, **43**:428–450, 2018, https://doi.org/10.1016/j.nonrwa.2018.03.010.
2. X. Chang, J. Zhang, Dynamics of a diffusive Leslie–Gower predator–prey system with ratio-dependent Holling III functional response, *Adv. Differ. Equ.*, **2019**:76, 2019, https://doi. org/10.1186/s13662-019-2018-3.
3. M. Chen, R. Wu, L. Chen, Spatiotemporal patterns induced by Turing and Turing-Hopf bifurcations in a predator-prey system, *Appl. Math. Comput.*, **380**:125300, 2020, https://doi.org/10.1016/j.amc.2020.125300.
4. R. Dáger, V. Navarro, M. Negreanu, Uniform boundedness for a predator-prey system with chemotaxis and dormancy of predators, *Q. Appl. Math.*, **79**(2):367–382, 2021, https://doi.org/10.1090/qam/1583.
5. L.N. Guin, P.K. Mandal, Spatial pattern in a diffusive predator–prey model with sigmoid ratio- dependent functional response, *Int. J. Biomath.*, . (05):1450047, 2014, https://doi.org/10.1142/S1793524514500478.
6. C. Ji, D. Jiang, X. Li, Qualitative analysis of a stochastic ratio-dependent predator–prey system, *J. Comput. Appl. Math.*, **235**(5):1326–1341, 2011, https://doi.org/10.1016/j.cam.2010.08.021.
7. W. Jiang, Q. An, J. Shi, Formulation of the normal form of Turing-Hopf bifurcation in partial functional differential equations, *J. Differ. Equations*, **268**(10):6067–6102, 2020, https://doi.org/10.1016/j.jde.2019.11.039.
8. P.H. Leslie, J.C. Gower, The properties of a stochastic model for the predator-prey type of interaction between two species, *Biometrika*, **47**(3/4):219–234, 1960, https://doi.org/10.2307/2333294.

9. X. Li, S. Ji, Existence of positive periodic solutions for a neutral impulsive predator-prey model with Crowley-Martin functional response, *Proc. Am. Math. Soc.*, **149**(11):4891–4906, 2021, https://doi.org/10.1090/proc/15593.

10. G. Liu, J. Yan, Positive periodic solutions of neutral predator–prey model with Beddington– Deangelis functional response, *Comput. Math. Appl.*, **61**(8):2317–2322, 2011, https://doi.org/10.1016/j.camwa.2010.09.067.

11. M. Liu, C. Du, M. Deng, Persistence and extinction of a modified Leslie–Gower Holling- type II stochastic predator–prey model with impulsive toxicant input in polluted environments, *Nonlinear Anal., Hybrid Syst.*, **27**:177–190, 2018, https://doi.org/10.1016/j.nahs.2017.08.001.

12. D. Luo, Q. Wang, Dynamic analysis on an almost periodic predator-prey system with impulsive effects and time delays, *Discrete Contin. Dyn. Syst., Ser. B*, **26**(6):3427, 2021, https://doi.org/10.3934/dcdsb.2020238.

13. P. Mishra, B. Tiwari, Drivers of pattern formation in a predator–prey model with defense in fearful prey, *Nonlinear Dyn.*, **105**(3):2811–2838, 2021, https://doi.org/10.1007/s11071-021-06719-2.

14. M. Qu, C. Zhang, X. Wang, Analysis of dynamic properties on forest restoration-population pressure model, *Math. Biosci. Eng.*, **17**(4):3567–3581, 2020, https://doi.org/10.3934/mbe.2020201.

15. S. Sasmal, Population dynamics with multiple Allee effects induced by fear factors – A mathematical study on prey-predator interactions, *Appl. Math. Modelling*, **64**:1–14, 2018, https://doi.org/10.1016/j.apm.2018.07.021.

16. H. Shi, S. Ruan, Y. Su, J. Zhang, Spatiotemporal dynamics of a diffusive Leslie– Gower predator–prey model with ratio-dependent functional response, *Int. J. Bifurcation Chaos Appl. Sci. Eng.*, **25**(05):1530014, 2015, https://doi.org/10.1142/S0218127415300141.

17. Q. Song, R. Yang, C. Zhang, L. Tang, Bifurcation analysis of a diffusive predator–prey model with Monod–Haldane functional response, *Int. J. Bifurcation Chaos Appl. Sci. Eng.*, **29**(11):1950152, 2019, https://doi.org/10.1142/S0218127419501529.

18. Y. Song, T. Zhang, Y. Peng, Turing–Hopf bifurcation in the reaction–diffusion equations and its applications, *Commun. Nonlinear Sci. Numer. Simul.*, **33**:229–258, 2016, https://doi.org/10.1016/j.cnsns.2015.10.002.

19. R.K. Upadhyay, S. Mishra, Population dynamic consequences of fearful prey in a spatio- temporal predator-prey system, *Math. Biosci. Eng.*, **16**(1):338–372, 2018, https://doi.org/10.3934/mbe.2019017.

20. L. Wang, C. Dai, M. Zhao, Hopf bifurcation in an age-structured prey-predator model with Holling III response function, *Math. Biosci. Eng.*, **18**(4):3144–3159, 2021, https://doi.org/10.3934/mbe.2021156.

21. L. Wang, W. Li, Periodic solutions and permanence for a delayed nonautonomous ratio- dependent predator–prey model with Holling type functional response, *J. Comput. Appl. Math.*, **162**(2):341–357, 2004, https://doi.org/10.1016/j.cam.2003.06.005.

22. X. Wang, L. Zanette, X. Zou, Modelling the fear effect in predator–prey interactions, *J. Math. Biol.*, **73**(5):1179–1204, 2016, https://doi.org/10.1007/s00285-016-0989-1.

23. X. Wang, X. Zou, Modeling the fear effect in predator–prey interactions with adaptive avoidance of predators, *Bull. Math. Biol.*, **79**(6):1325–1359, 2017, https://doi.org/10.1007/s11538-017-0287-0.

24. H. Zhang, Y. Cai, S. Fu, W. Wang, Impact of the fear effect in a prey-predator model incorporating a prey refuge, *Appl. Math. Comput.*, **356**:328–337, 2019, https://doi.org/10.1016/j.amc.2019.03.034.

25. J. Zhao, H. Zhang, J. Yang, Stationary patterns of a ratio-dependent prey-predator model with cross-diffusion, *Acta Math. Appl. Sin., Engl. Ser.*, **33**(2):497–504, 2017, https://doi.org/10.1007/s10255-017-0677-y.